Noname manuscript No.
(will be inserted by the editor)

A fractional nonlocal approach to nonlinear blood flow in small-lumen arterial vessels

Gioacchino Alotta · Mario Di Paola · Francesco Paolo Pinnola · Massimiliano Zingales

Received: date / Accepted: date

Abstract The behavior of human blood flowing in arteries is still an open topic for its multi-phase nature and heterogeneity. In large arterial vessels the well-known Hagen-Poisueille law, which main assumption is that the blood is Newtonian, is considered acceptable. In small arterial vessels, instead, this law does not reproduce experimental results that show non-parabolic profiles of velocity across the vessel diameter. For capillary vessels the Casson model of fluids that is nonlinear is used in place the Newton law, resulting in nonlinear governing equations and difficulties in mathematical manipulation. For these reasons an alternative approach is proposed in this paper. Starting from the micro-mechanics of blood, the Hagen-Poisueille model is enriched with long-range interactions that simulate the interactions of non-adjacent fluid volume elements due to the presence of red blood cells and other dispersed cells in the plasma. These nonlocal forces are defined as linearly dependent on the product of the volumes of the considered elements and on their relative velocity. Moreover, as the distance between two volume elements increases, the nonlocal forces are scaled through an attenuation function; if this function is chosen as a power law of real order of the distance between the volume elements, an operator related to the fractional derivative of relative velocity appears in the resulting governing equation. It is

G. Alotta
Dipartment of Civil, Energy, Environment and Materials Engineering (DICEAM), University "Mediterranean" of Reggio Calabria, ReggioCalabria, Italy.
E-mail: gioacchino.alotta@unirc.it

M. Di Paola
Department of Engineering (DI), Univeristy of Palermo, Viale delle Scienze Ed. 8 90128, Palermo, Italy
E-mail: mario.dipaola@unipa.it

F. P. Pinnola
Department of Structures for Engineering and Architecture (DIST), University of Naples "Federico II", Naples, Italy
E-mail: francescopaolo.pinnola@unina.it

M. Zingales
Department of Engineering (DI), Univeristy of Palermo, Viale delle Scienze Ed. 8 90128, Palermo, Italy
E-mail: massimiliano.zingales@unipa.it

shown that the fractional Hagen-Poisueille law is able to reproduce experimentally measured profiles of velocity with a great accuracy, moreover as the dimension of the vessel increases, nonlocal forces become negligible and the proposed model reverts to the classical Hagen-Poisueille model.

Keywords Blood flow · nonlocal fluid · Mesoscale approach · fractional model

1 Introduction

The rheological behavior of blood has been investigated from the nineteenth century and it is still an open debate. Indeed the characteristic of blood flow inside vessels strongly affects stresses that are transmitted by the blood to the vessels themselves; in a biomechanics context, stresses on the vessels may be determinant for some arterial widespread diffused diseases such as aneurysm or for consequences of arterial stenosis. For these reasons, analytical models capable to accurately predict the main features of blood flow inside human arteries are essential in order to better understand the mechanisms of appearance of aneurysms and consequence in blood supply downstream the aneurysm or a stenosis; moreover, an accurate description of blood flow is essential in order to allow the definition of medical protocols able to predict the evolution of an aneurysm on the basis of medical images. The first model for blood flow inside arterial vessels is the well-known Hagen-Poiseuille (HP) law [1], derived assuming Newtonian fluid and providing parabolic profile of velocity along the diameter of a circular vessel; this model has proven to be reliable for large arterial vessels [1,2]. For capillary arterial vessels experimentally measured profiles of velocity are not parabolic [3], hence the HP model is not suitable for this kind of problem. In the case of capillary vessels the Casson model is certainly more reliable of the HP; this law considers a nonlinear relationship between shear stress and shear rate with the introduction of the concept of yield stress of the fluid that leads to a nonlinear governing equation and piece-wise profile of velocity across the vessel diameter. The Casson law provides results in good agreement with experimental observations, however mathematical manipulations are not straightforward due to the nonlinearity and the model is not obtained on physical evidences on the mechanics of blood flow. An alternative and effective approach to nonlinear modeling of blood is represented by the nonlocal approach.

Nonlocal mechanics, both in terms of gradients [4,5,6,7] or integrals [8,9,10] of the state variables of the problem, has proved to be effective in modeling a wide range of solid mechanics problems such as wave dispersion, shear bands as well as strain localization in mechanical interfaces [11,12], but also to take into account for heterogeneity in the medium at hands. In the context of fluid mechanics, nonlocal theories have been proposed to capture the motion of fluids in microvessels or in order to perform efficient simulation of fluid with dispersion [13,14,15,16,17,18]. In the approaches available in literature, however, the nonlocal interactions are not constructed on solid mechanical basis. For the above-mentioned reasons, in this paper an alternative mesoscale approach is proposed. The model is based on the HP law that is enriched with nonlocal forces mutually exerted by non-adjacent fluid elements; these forces are transmitted to relatively long distance by relatively large cells, mainly Red

Blood Cells (RBC). These long-range interactions are constructed as volume viscous forces scaled by an attenuation function that decreases the forces mutually exerted by two non-adjacent volume elements as the distance between them increases; the approach is analogous of that successfully used in various micro/nanomechanics problems [19,20,21,22,23,24]. As a consequence in the governing equation an integral representing these additional forces appears; it is shown that if the attenuation function is chosen as a power law of the distance between two volume elements, the integral representing non local forces is closely related to a fractional derivative operator [25,26] (or it is exactly a fractional derivative if unbounded domains are considered). The advantage of this formulation is that the governing equation remains linear and comparison with experimentally observed velocity profiles along capillary vessels diameter shows very good agreement, with lower root mean square error in comparison with Casson model. The model is able to automatically reverts to the classical Hagen-Poiseuille law when the vessel is not capillary, indeed as the diameter of the vessel increases nonlocal forces become negligible. Moreover it is shown that the model is able to numerically reproduce the shear thinning behavior of blood observed in rotating viscometer.

2 Governing equation of nonlocal flow

In this section the equations governing the fluid motion are briefly described. In Sec. 2.1 the Navier-Stokes equations for Newtonian uncompressible fluids are recalled, while in Sec. 2.2 the gradient and integral approaches to nonlocality are briefly described and finally the proposed mechanically based approach to nonlocality is introduced in Sec. 2.3.

2.1 Navier-Stokes equations (local)

The dynamic equilibrium of a generic fluid element is completely described by enforcing the linear momentum balance and the balance of mass. The equation of the linear momentum balance, describing the dynamic equilibrium of a fluid element, may be written as follows:

$$\rho(\boldsymbol{x},t)\boldsymbol{f}(\boldsymbol{x},t)-\frac{\mathrm{D}\rho(\boldsymbol{x},t)\boldsymbol{v}(\boldsymbol{x},t)}{\mathrm{D}t}+\mathrm{div}\boldsymbol{T}(\boldsymbol{x},t)=0 \tag{1}$$

where $\rho(\boldsymbol{x},t)$ is the density, $\boldsymbol{f}(\boldsymbol{x},t)$ is the volume forces vector, $\boldsymbol{v}(\boldsymbol{x},t)$ is the velocity vector, D/Dt is the total derivative operator, $\boldsymbol{T}(\boldsymbol{x},t)$ is the Cauchy stress tensor, $\boldsymbol{x}$ is the position vector and t is the time. Eq. (1) is a set of three coupled partial differential equations in the unknown fields $\boldsymbol{v}(\boldsymbol{x},t)$, $\boldsymbol{T}(\boldsymbol{x},t)$ and $\rho(\boldsymbol{x},t)$; they describe the dynamic equilibrium along three mutually orthogonal directions.
To the purpose of solving the system in Eq. (1) the constitutive behavior of the fluid at hands must be introduced. In particular, the Navier-Stokes equation are related to uncompressible Newtonian fluid. From the uncompressibility hypothesis descends that $\rho(\boldsymbol{x},t)=\rho$. A Newtonian fluid is such that the deviatoric component of the stress

tensor is directly proportional to the strain rate tensor $\dot{\boldsymbol{\varepsilon}}_D$ and for this reason the stress tensor may be written as in the following:

$$\boldsymbol{T}(\boldsymbol{x},t) = p(\boldsymbol{x},t)\boldsymbol{I} + 2\mu\dot{\boldsymbol{\varepsilon}}_D(\boldsymbol{x},t) \tag{2}$$

where the first term of the rhs is the volumetric part of the stress tensor and the second term is the deviatoric part, p is the pressure, $\boldsymbol{I}$ is the identity matrix and μ is the dynamic viscosity. The strain rate tensor $\boldsymbol{\varepsilon}_D$ may be written in terms of the velocity field $\boldsymbol{v}(\boldsymbol{x},t)$ by means of the compatibility equations as follows:

$$\dot{\varepsilon}_{D,ij} = \frac{1}{2}\left(\frac{\partial v_i}{\partial x_j} + \frac{\partial v_j}{\partial x_i}\right) - \frac{\dot{\theta}}{3}\delta_{ij}; \quad i,j = 1,2,3; \tag{3}$$

being $\dot{\varepsilon}_{D,ij}$ the element in the i-th row and the j-th column of $\dot{\boldsymbol{\varepsilon}}_D$, v_i the i-th component of the velocity vector, x_i the i-th axis in the coordinate system and $\dot{\theta}$ the volumetric strain rate. By inserting Eq. (2) and Eq. (3) into Eq. (1) and taking into account of the uncompressibility condition the Navier-Stokes equations are obtained in the following form:

$$\rho\frac{\mathrm{D}\boldsymbol{v}(\boldsymbol{x},t)}{\mathrm{D}t} - \nabla p(\boldsymbol{x},t) - \mu\nabla^2\boldsymbol{v}(\boldsymbol{x},t) - \rho\boldsymbol{f}(\boldsymbol{x},t) = 0 \tag{4}$$

in the unknown velocity field $\boldsymbol{v}(\boldsymbol{x},t)$ and in the unknown pressure field $p(\boldsymbol{x},t)$. In order to obtain the solution, it is necessary to enforce the balance of mass that, for uncompressible fluids, reads:

$$\mathrm{div}\boldsymbol{v} = 0 \tag{5}$$

that is commonly known as *continuity equation*. Note that Eq. (5) has been also considered in the substitution of the compatibility equations inside the linear momentum balance Eq. (1). The Navier-Stokes equations are the basis of the fluid mechanics, however they are not satisfactory in describing multiphase or microstructured fluid such as the blood. For this reason researchers of the field have made a great effort in the last decades in order to formulate models capable to predict more accurately the blood behavior.

2.2 Nonlocal models

In the last decades many nonlocal models have appeared in literature with applications both in the field of solid mechanics and in field of fluid mechanics. These models may be subdivided into two main categories, that are gradient or weak nonlocal models and integral or strong nonlocal models. We will briefly recall both kind of nonlocal models in the following.
In gradient nonlocal models the stress tensor is the sum of the Cauchy stress and of the second order gradient of the stress; the constitutive law may be written as follows:

$$\boldsymbol{\sigma}(\boldsymbol{x},t) = \boldsymbol{T}(\boldsymbol{x},t) - \nabla^2\boldsymbol{T}(\boldsymbol{x},t)l_c^2 \tag{6}$$

where $\boldsymbol{\sigma}(\boldsymbol{x},t)$ is the total stress tensor, while $\nabla^2\boldsymbol{T}(\boldsymbol{x},t)$ is the so-called higher order stress tensor that is the work conjugate of the strain gradient (for solid or strain rate gradient for fluid) tensor that represents the nonlocal part of the stress tensor and l_c is a specific internal scale. Constitutive models of the type of Eq. (6) have been applied successfully in the study of many engineering problems, such as nonlocal effects, dislocation kinematics, the formation of shear bands and also during the plastic deformations of metals and to eliminate singularities at dislocation lines and crack tips [27]. Mathematical manipulations in presence of the constitutive equation (6) is very cumbersome, then many authors have put their effort to obtain simplified formulations able to reproduce the same results of Eq. (6) (see for example [28]). Recently, microstructured fluid have been investigated in the context of gradient models of mechanics [29] introducing a nonlocal model of Herschal-Bulkey relation that reads in our particular study:

$$< |t_{rz}| - l_c^2 \frac{d^2|t_{rz}|}{dr^2} - \tau_0 >= \mu^{1/n} |\dot{\gamma}_{rz}|^n \tag{7}$$

where $< x >= \frac{x+|x|}{2}$ is the positive operator, n is a non-Newtonian dependence on the material flow rate, τ_0 is the initial yield stress, t_{rz} is the shear stress in the direction of the fluid flow (z), r is the radial coordinate and γ_{rz} is the shear strain. The flow transport equation in Eq. (7) is a nonlocal gradient generalization of linear nonlocal approach ([27]) with the introduction of a nonlocal stress as ($\tau_0 = 0$, $n = 1$):

$$t_{rz} - l_c^2 \frac{d^2 t_{rz}}{dr^2} - \tau_0 = \mu \dot{\gamma}_{rz} = \mu \frac{dv_z}{dr} \tag{8}$$

being v_z the velocity in the flow direction, that can be compared with the well-known stress gradient approaches to nonlocal solid mechanics in 1D reading [28]:

$$t_{rz}^{(l)} + t_{rz}^{(nl)} = E\gamma_{rz} \tag{9}$$

where E is the elastic modulus and the nonlocal stresses $t_{rz}^{(nl)} = -l_c^2 \frac{d^2 t_{rz}}{dz^2}$ is related to the local contribution by the second order gradient operator. The constitutive assumption in Eq. (8) may be considered in the balance equation to yield, upon the integration, the velocity profile of the microstructured fluid [14,15,29].
In integral models the equilibrium of a solid or fluid elements involves terms depending on the integral over the domain of the strain (or strain rate for the case of fluid). The first to propose such a kind of strong nonlocal model was Eringen [8] regarding solid mechanics problems and many modifications appeared in literature after the paper [8] in order to adapt it to various engineering and physical problems. A general integral nonlocal model may be written as follows:

$$\boldsymbol{\sigma}(\boldsymbol{x},t) = \boldsymbol{T}(\boldsymbol{x},t) + \int_V g(\boldsymbol{x} - \boldsymbol{\xi}) \boldsymbol{\varepsilon}(\boldsymbol{\xi},t) d\boldsymbol{\xi} \tag{10}$$

where $g(\cdot)$ is the Kroner-Eringen attenuation function, $\boldsymbol{x}$ and $\boldsymbol{\xi}$ are the positions of the interacting volume elements and $\boldsymbol{\varepsilon}$ is the strain tensor. Eq. (10) is particularized for nonlocal elasticity. Integral approach to fluids nonlocality have been proposed in recent papers (see e.g. [18]) assuming that the relations among the shear stress and shear strain are of the type of Eq. (10) where the strain tensor $\boldsymbol{\varepsilon}$ has been substituted with the strain rate tensor $\boldsymbol{\varepsilon}_D$. Examples of strong nonlocality applied to fluid

mechanics can be also found in [13,14,15]. Despite the wide diffusion of integral nonlocal elasticity and viscosity models, they show mathematical inconsistencies as bounded domains are considered [19]; indeed in this case the presence of nonlocal interactions involves the appearance of constitutive boundary conditions that violate the equilibrium [30].
These considerations push toward a different approach to nonlocal viscosity model as proposed in the next sections.

2.3 Mechanically based nonlocality

In the last years the authors of the present paper developed an alternative approach to nonlocal models described above for nonlocal-elasticity [19,21,22,23,24]. In this approach, the nonlocal forces are constructed on a mechanical basis by inserting in the model long-range springs such that non-adjacent volume elements mutually exchange forces due to relative motion. In the case of fluids, the mechanics of long-range interactions is assumed Newtonian and the resultant of nonlocal viscous forces applied (see Fig. 1) to a generic volume element reads:

$$\boldsymbol{f}_v^{(nl)}(\boldsymbol{x},t) = \int_V \boldsymbol{f}_v^{(nl)}(\boldsymbol{x},\boldsymbol{\xi},t) = dV(\boldsymbol{x}) \int_V \boldsymbol{G}_v\,(\boldsymbol{x}-\boldsymbol{\xi})\,(\boldsymbol{v}(\boldsymbol{\xi},t)-\boldsymbol{v}(\boldsymbol{x},t))\,dV(\boldsymbol{\xi}) \quad (11)$$

where $\boldsymbol{f}_v^{(nl)}(\boldsymbol{x},\boldsymbol{\xi},t)$ is the nonlocal viscous force applied to volume element located at $\boldsymbol{x}$ due to the relative velocity with the volume element located at $\boldsymbol{\xi}$, $\boldsymbol{G}_v\,(\boldsymbol{x}-\boldsymbol{\xi}) = g\,(\boldsymbol{x}-\boldsymbol{\xi})\,[\boldsymbol{I}-\boldsymbol{J}(\boldsymbol{x},\boldsymbol{\xi})]$, being $g\,(\boldsymbol{x},\boldsymbol{\xi})$ the attenuation function and $\boldsymbol{J}\,(\boldsymbol{x},\boldsymbol{\xi})$ the Jacobi directional tensor which components are written as $J_{kj}\,(\boldsymbol{x},\boldsymbol{\xi}) = i_k\,(\boldsymbol{x},\boldsymbol{\xi})\,i_j\,(\boldsymbol{x},\boldsymbol{\xi})$, where $i_k\,(\boldsymbol{x},\boldsymbol{\xi})$ is the $k-th$ component of the unit vector in the direction $(\boldsymbol{x}-\boldsymbol{\xi})$ defined as:

$$i_k\,(\boldsymbol{x},\boldsymbol{\xi}) = \frac{(\xi_k - x_k)}{|\boldsymbol{i}\,(\boldsymbol{x},\boldsymbol{\xi})\,|} \quad (12)$$

The attenuation or decay function $g\,(\boldsymbol{x}-\boldsymbol{\xi})$ is a symmetric and real function that decays with the distance.
In the case of the human blood the nonlocal forces in Eq. (11) are introduced for its multiphase nature and the tendency to self organize in a microstructure. Such a kind of microstructures are mainly constituted by RBCs that are considered to be the most responsible for the non-Newtonian behavior of blood. Indeed they aggregates into the so-called Rouleaux formations (see Fig. 2); moreover, RBCs have the tendency to migrate toward the center of the arterial vessels (Fahereus-Lindqvuist wall effect, see Fig. 3). In small arterial vessels these two phenomena are able to modify the whole blood behavior, while in large arterial vessels their influence is negligible.This fact highlights the size-dependent behavior of the blood flow. In order to perform reliable and computationally efficient biomechanical simulations for cardiovascular applications, the blood domain is considered homogeneous and its heterogeneity and microstructure is accounted by means of the long-range viscous forces introduced in Eq. (11). Indeed the simulation of liquid phase and corpuscle require high computational efforts.

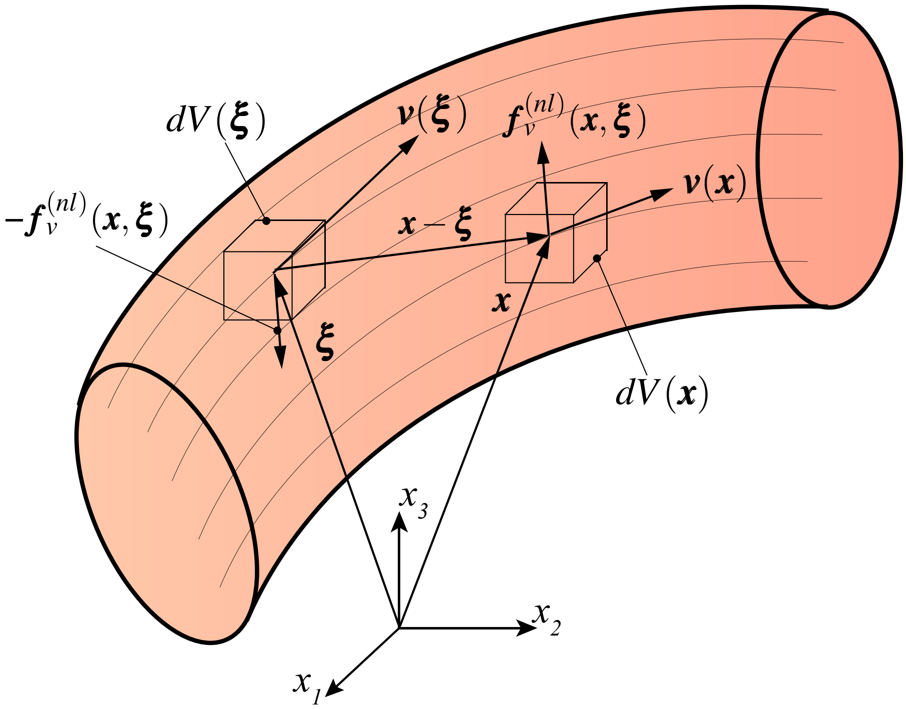

Fig. 1 Nonlocal forces mutually exerted by two non-adjacent volume forces are proportional to the difference of velocity vectors.

The nonlocal Navier-Stokes equations are written starting from the linear momentum balance, by including the local constitutive behavior Eq. (2), introducing the non local forces of Eq. (11) and taking into account uncompressibility condition as:

$$\rho\left(\frac{\partial \boldsymbol{v}(\boldsymbol{x},t)}{\partial t}+\boldsymbol{v}(\boldsymbol{x},t)\cdot\nabla\boldsymbol{v}(\boldsymbol{x},t)\right)-\nabla p(\boldsymbol{x},t)-\mu\nabla^2\boldsymbol{v}(\boldsymbol{x},t)+$$
$$-\int_V \boldsymbol{G}_v(\boldsymbol{x}-\boldsymbol{\xi})\left(\boldsymbol{v}(\boldsymbol{\xi},t)-\boldsymbol{v}(\boldsymbol{x},t)\right)dV(\boldsymbol{\xi})-\rho\boldsymbol{f}(\boldsymbol{x},t)=0 \quad (13)$$

Eq. (13) corresponds to Eq. (4) with the additional integral terms representing the resultant of nonlocal forces. Inspection of Eq. (13) reveals that the nonlocal force between two volume elements is defined in the direction of the component of the vector $[\boldsymbol{v}(\boldsymbol{\xi},t)-\boldsymbol{v}(\boldsymbol{x},t)]$ perpendicular to $(\boldsymbol{x}-\boldsymbol{\xi})$.

3 Mesoscale model of the Poiseuille flow

In this section Eq. (13) is particularized to the case of the 1D axisymmetric flow in stationary conditions. Let us consider a cylindrical volume $V = AL$, where L is the length in the direction of the axis of the cylinder and A the cross sectional area of the

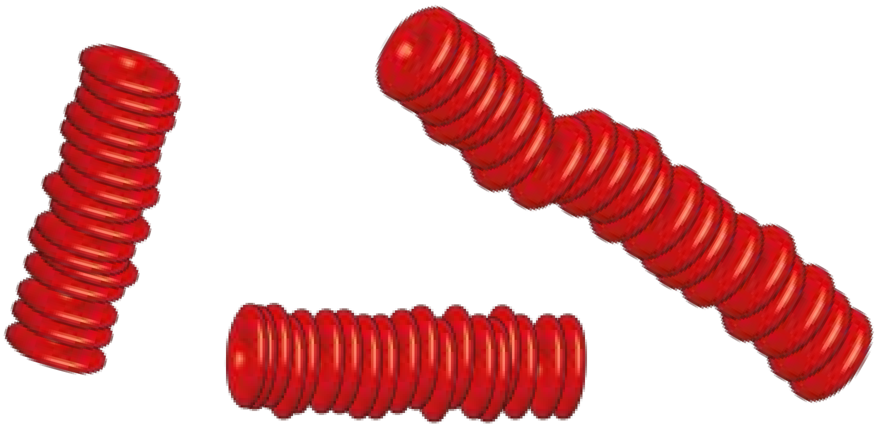

Fig. 2 Rouleaux formations.

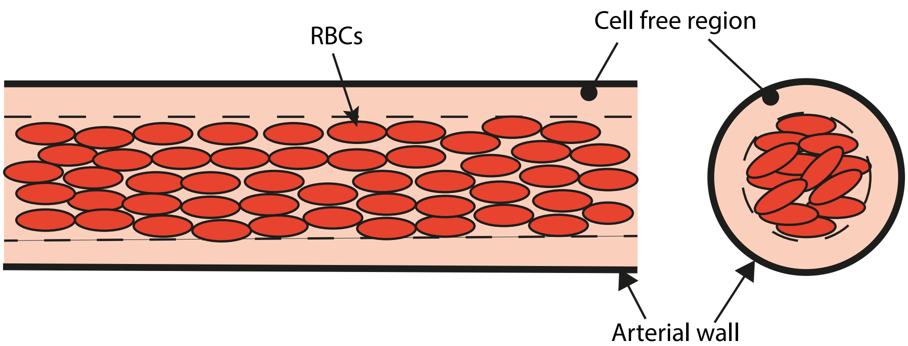

Fig. 3 Fahraeus-Lindqvist wall effect.

considered domain. Volume V is referred to a cylindrical coordinate system (r,θ,z) as reported in Fig. 4 and let us assume that a pressure drop of $\Delta p = p(r,\theta,0) - p(r,\theta,L)$ is applied at the two sides of the cylinder. In such circumstances the linear momentum balance on a volume element Fig. 4b along the flux direction (z) reads:

$$\begin{aligned}&[t_{zz}(r,\theta,z+\Delta z) - t_{zz}(r,\theta,z)]\,r\Delta\theta\Delta r + [t_{\theta z}(r,\theta+\Delta\theta,z) - t_{\theta z}(r,\theta,z)]\,\Delta z\Delta r + \\ &\qquad t_{rz}(r+\Delta r,\theta,z)(r+\Delta r)\Delta z\Delta\theta - t_{rz}(r,\theta,z)r\Delta z\Delta\theta = \frac{\mathrm{D}\rho v_z}{\mathrm{D}t} r\Delta z\Delta\theta\Delta r \qquad (14)\end{aligned}$$

being ρ the fluid density $\rho(r,\theta,z,t)$ and $\frac{\mathrm{D}}{\mathrm{D}t}$ the total derivative operator. Eq. (14) may be rewritten, after some straightforward manipulations, as:

$$\frac{\partial t_{rz}}{\partial r} + \frac{t_{rz}}{r} + \frac{1}{r}\frac{\partial t_{\theta z}}{\partial \theta} + \frac{\partial t_{zz}}{\partial z} = \frac{\mathrm{D}\rho v_z}{\mathrm{D}t} \qquad (15)$$

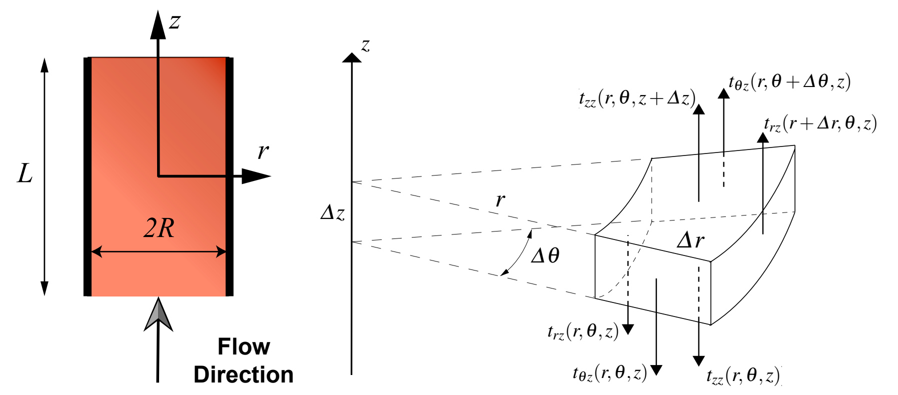

(a) (b)

Fig. 4 Blood vessel model.

Under the assumptions of axisymmetric flow and stationary flow ($\mathrm{D}\rho v_z/\mathrm{D}t = 0$) the balance equation in Eq. (15) yields:

$$\frac{\partial t_{rz}}{\partial r} + \frac{t_{rz}}{r} = -\frac{\partial t_{zz}}{\partial z} = -\frac{\Delta p}{L} \tag{16}$$

where we assumed that the pressure gradient is constant from $z = 0$ to $z = L$. Eq. (16) is a differential equation in the unknown shear stress $t_{rz}(r)$; in order to be solved it is necessary to enforce the rheological behavior, that in the case of Newtonian fluid reads:

$$t_{rz} = \mu \frac{\partial v_z}{\partial r} = \mu \frac{\partial}{\partial t}\frac{\partial u_z}{\partial r} = \mu \dot{\gamma}_{rz} \tag{17}$$

where $\dot{\gamma}_{rz}$ is the shear rate, that is the rate of the change of the displacement $u_z = u_z(r)$ of the generic particle inside the control volume. Eq. (17) is a constitutive equation that relates the shear stress to the shear rate in the actual configuration of the fluid, and, after substitution, we get:

$$\mu \frac{d^2 v_z}{dr^2} + \frac{\mu}{r}\frac{dv_z}{dr} = -\frac{\Delta p}{L} \tag{18a}$$

$$v_z(-R) = 0; \qquad v_z(R) = 0 \tag{18b}$$

being R the radius of the cylinder, that may be solved with the additional boundary conditions in Eq. (18b) for the velocity at the border of the domain to yield:

$$v_z(r) = \frac{R^2 - r^2}{4\mu}\frac{\Delta p}{L} \tag{19}$$

that describes a parabolic velocity profile along the diameter of the considered circular cross-section. It is to emphasize that the equation in Eq. (18a) may be obtained directly by particularizing Eq. (4).

3.1 Small capillary vessels

In small-diameter vessels the experimental evidences [3] show a strong deviation from the parabolic profile predicted by assuming the Newtonian constitutive equation. Such a discrepancy, observed at the beginning of the fifties of last century is probably due to Fahreius-Lindqvist effect (Fig. 3) and Rouleaux formations (Fig. 2) already described in the previous section. The constitutive model capable to reproduce the experimental measured velocity profiles is the so-called Casson model, that reads:

$$\sqrt{t_{rz}(r)} = \sqrt{\tau_0} + \sqrt{\mu}\,(\dot{\gamma}_{rz})^{1/2} \tag{20}$$

Eq. (20) is a nonlinear relationship between shear stress and shear rate. If $\tau_0 = 0$ it reverts to the Newtonian model of Eq. (17). Introducing Eq. (20) into the balance equation in Eq. (16), a nonlinear governing equation is obtained:

$$-\frac{\Delta p}{L} = \frac{1}{r}\left[\tau_0 + \mu\frac{du_z}{dr} + 2\sqrt{\tau_0\mu}\left(\frac{du_z}{dr}\right)^{\frac{1}{2}}\right] + \frac{d^2u_z}{dr^2}\left[\mu + 2\sqrt{\tau_0\mu}\left(\frac{du_z}{dr}\right)^{-\frac{1}{2}}\right] \tag{21}$$

The solution to Eq. (21) is a piece-wise velocity profile that may be expressed in the form:

$$\begin{aligned} u_z(r) =& \frac{R^2}{4\mu}\left\{\frac{\Delta p}{L}\left[1-\left(\frac{r}{R}\right)^2\right] - \frac{8}{3}\left(\frac{2\tau_0}{R}\frac{\Delta p}{L}\right)^{\frac{1}{2}} \times \right. \\ & \left. \left[\left(1-\frac{r}{R}\right)^{\frac{3}{2}}\right] + \frac{4\tau_0}{R}\left(1-\frac{r}{R}\right)\right\} \qquad |r| > r_y \end{aligned} \tag{22a}$$

$$u_z(r) = u_z(r_y) \qquad |r| \le r_y \tag{22b}$$

where $r_y = (2\tau_0 L)/\Delta p$. From the inspection of Eq. (22) we find that in the central part of the vessel, the velocity is constant; this is related to the fact that in the region $-r_y \le r \le r_y$ the yield stress τ_0 is not exceeded, hence the velocity gradient is zero. The Casson model is satisfying in the reproduction of non-Newtonian velocity profiles, however it has the disadvantage to be nonlinear, hence mathematical manipulations are not straightforward except that for simple problems (see e.g. [2]), such as the case of the Poiseuille flow studied in this section. Moreover the concept of shear yield stress, in the authors opinion, does not reflect the real mechanics of the blood flow, that is not a visco-plastic fluid but it is a multiphase medium. For these reasons, in the next sections an alternative approach is proposed.

3.2 Mesoscale approach to blood circulation in small-size arterial vessels

In this section the nonlocal blood flow model is introduced starting from simple observations regarding the mechanics of blood. In particular two main facts are taken into account:

- the blood is multiphase material, which contains a fluid part, the plasma, and many different solid parts, such as RBCs that are the larger and more influent cells;

– the blood is strongly heterogeneous, indeed the presence of the Fahraues-Lindqvuist wall effect (see Fig. 3) and Rouleaux formations(see Fig. 2) make the concentration of RBCs larger at the center of the vessels than at the sides; as a consequence if the dimensions and the position of a representative volume are changed, different situations may be found.

In order to take into account of these peculiarities without really modelling all the phases contained in the blood, it is possible to adopt a *mesoscale approach*. In this manner, the blood is considered as a homogeneous fluid and the presence of RBCs and fibrinogen is taken into account by inserting in the governing equations long-range forces mutually exerted by non-adjacent fluids elements. The reason to introduce these forces is readily understandable if Fig. 5 is closely inspected. Indeed when

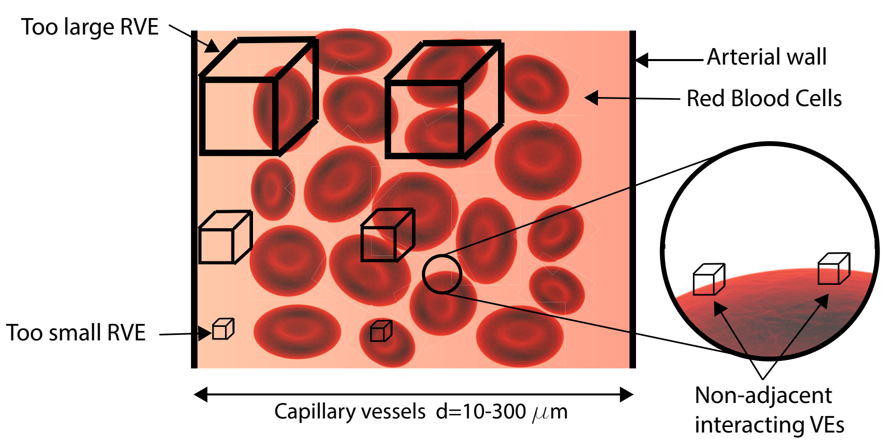

Fig. 5 Heterogeneity and multiphase nature of blood. In the circle, two non-adjacent fluid elements mutually exchange forces because of the presence of the RBC.

the dimension of the vessel is comparable to the average dimension of RBCs, that is about 7.5 μm, a Representative Volume Elements (RVE) that is suitable for the dimension of the domain is too small because it is not really representative of all heterogeneity of the blood; on the contrary, an RVE sufficiently large to be representative of the heterogeneous nature of blood is too large because its dimensions are of the same order of magnitude of the domain dimension. Then, in the framework of a mesoscale approach, if two very small volume elements are taken on the boundary of a RBC, it is reasonable to think that they interact because of the presence of the RBC itself, and their interaction is modeled here as a nonlocal viscous force. In particular nonlocal forces are thought as linearly depending on the product between the two interacting volumes and their relative velocity; moreover the long-range forces are weighted by an attenuation function that decreases the force magnitude as the distance between the two elements increases. Under these assumptions the force mutually exerted by two non-adjacent volume elements may be written as follows for a one-dimensional problem (see Fig. 6):

$$F_{ki} = \mu_{ki} \Delta V_k \Delta V_i (v_i - v_k) \tag{23}$$

where ΔV_k and ΔV_i are the volume of the two fluid elements, while v_k and v_i are the velocities of the fluid elements; μ_{ki} is a viscous coefficient that varies with the distance d_{ki} through an appropriate attenuation function $g(\cdot)$, that is $\mu_{ki} = \mu_{NL} g(d_{ki})$, being μ_{NL} a nonlocal viscosity parameter of the model. The nonlocal viscosity μ_{NL}, together with the attenuation function $g(\cdot)$, governs the entity of long-range viscous forces. It may be thought as the nonlocal counterpart of the local viscosity μ. For fixed local viscosity μ and attenuation function $g(\cdot)$ a larger value of μ_{NL} implies a larger intensity of nonlocal interactions compared with the local ones and then a major deviation from the local behavior of the fluid. Its physical meaning may be defined with the following parallelism: as the local viscosity fluid μ reflects the capability of the fluid volume to "drag" adjacent volume elements, the nonlocal viscosity μ_{NL} quantifies the capability of the fluid volume to "drag" non-adjacent volume elements. The resultant of nonlocal forces on the element k may be written as follows:

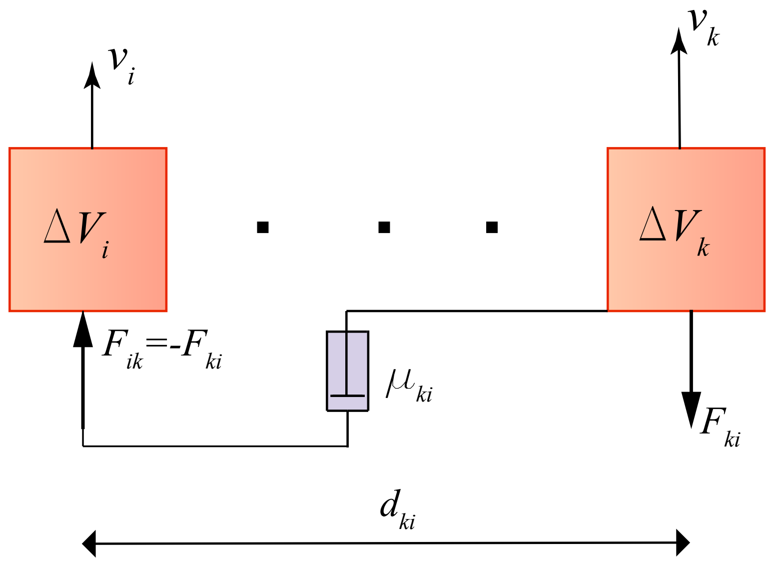

Fig. 6 Nonlocal forces mutually exerted by the two volume elements i and k in a one-dimensional problem.

$$F_k = \mu_{NL} \Delta V_k \sum_{i=1}^{N} \Delta V_i g(d_{ki})(v_i - v_k) \tag{24}$$

being N the number of element in which the domain is discretized. If we refer to the two dimensional domain of Fig. 7 in axisymmetric conditions, the resultant of nonlocal forces on the $k-th$ volume element may be written as:

$$F_k = \mu_{NL} \Delta V_k \sum_{i=1}^{N_r} \sum_{j=1}^{N_\theta} \Delta V_{ij} g(d_{k,ij})(v_{ij} - v_k) \tag{25}$$

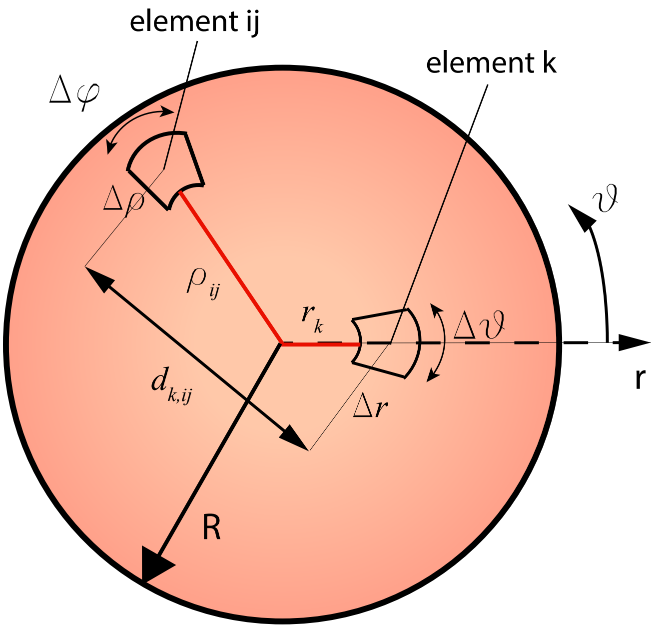

Fig. 7 Two dimensional axisymmetric domain (cross section of the circular vessel).

where:

$$\Delta V_k = r_k \Delta r \Delta \theta L \qquad \Delta V_{ij} = \rho_{ij} \Delta \rho \Delta \varphi L \tag{26}$$

are the volumes of the two considered fluid elements and N_r and N_θ are the number of elements in which the radial and circumferential directions have been discretized, respectively. By taking the limits for $\Delta V_k \to 0$ and $\Delta V_{ij} \to 0$, the double sum reverts to a double integral as:

$$F(r) = \mu_{NL} \int_0^R \int_0^{2\pi} g(d_{r\theta,\rho\varphi}) \left(v(\rho) - v(r)\right) \rho d\varphi d\rho \tag{27}$$

where the dependence of F, $v(r)$ and $v(\rho)$ from the angular coordinates θ and φ has intentionally been omitted because the problem is axisymmetric, while for obvious geometric reasons the same can not be done for $g(d_{r\theta,\rho\varphi})$, being $d_{r\theta,\rho\varphi}$ the distance between two generic volume elements. As for the attenuation function, typical forms are exponential, power law or Gaussian; in this study a power law attenuation function in the form:

$$g(d_{r\theta,\rho\varphi}) = \frac{1}{(d_{r\theta,\rho\varphi})^{2+\alpha}} \tag{28}$$

has been selected; in Eq. (28) $d_{r\theta,\rho\varphi} = \sqrt{\rho^2 + r^2 - 2r\rho\cos\varphi}$ and α is a parameter governing the velocity of decaying of the entity of long-range interactions as the distance increases; with these assumptions the governing equation is obtained as:

$$-\frac{\Delta p}{L} = \mu \left(\frac{1}{r}\frac{dv(r)}{dr} + \frac{d^2 v(r)}{dr^2} \right) + \mu_{NL} L \int_0^R \int_0^{2\pi} \frac{(v(\rho) - v(r))}{(\rho^2 + r^2 - 2r\rho\cos\varphi)^{\frac{2+\alpha}{2}}} \rho d\varphi d\rho \tag{29}$$

which may be labelled as *Fractional Hagen-Poiseuille* (FHP) law, since the integral term is strictly related to the Marchaud fractional derivative in polar coordinates (see Appendix and [26,31]). From a rigorous point of view a proper fractional operator is not present in Eq. (29). Indeed in a bounded domain, as in the considered application, a properly said fractional operator would involve additional non integral terms, as in the case of Eqs. (37) of the Appendix (for one-dimensional problem). From a mechanical point of view these additional terms have not correspondence, except if we admit the presence of long-range viscosity connecting volume elements with the frontier, analogously to the approach followed in [32] in the case of nonlocal elasticity. However in our mechanical representation these long-range interactions between volume elements and the bounds of the domain are not present and then the additional terms related to fractional derivative in bounded domain do not appear. But if the domain was unbounded, the integral in Eq. (29) would be a two-dimensional Central Marchaud fractional derivative (see Appendix) in polar coordinates and for this reason we feel that the present formulation may be labeled as “fractional”.
The solution of such a problem in analytical form is not straightforward and it may be found for a restricted class of problem, such as very simple geometry with no real engineering relevance (e.g. unbounded domains); however, accurate solutions may be easily found by discretizing the domain and the governing equation with a finite difference approximation. The advantage on the use of the proposed approach compared with the gradient or Eringen integral approaches is that the boundary conditions can be enforced as in a problem involving a classical local fluid [19]; then the boundary conditions are exactly the same of those in Eq. (18b) that in the context of a finite difference approximation are enforced in a straightforward manner. In the next section, Eq. (29) is used in order to fit experimental data and the simulate velocity profiles in a small arterial vessel.

3.3 Best fitting of model parameters

In [3] results of measurements of velocity profiles on arterioles of rabbit mesentery have been reported. The data refers to arterioles with diameter size in the range 17-32 μm. In this study data obtained on a 32 μm diameter vessels (Fig. (3) of Ref. [3]) have been used in order to calibrate parameters of the HP model, the Casson model and the proposed fractional nonlocal model. For the HP and the Casson models the least squares method has been used in order to calibrate the mechanical parameters. For the FHP model, since analytical solution for the Poiseuille flow is not available, the parameters have been calibrated by means of an iterative procedure. In this procedure the discretized version of Eq. (29) has been solved numerically several times with different set of parameters. At the end of the procedure, the adopted parameters are those that minimize the Root Mean Square Error (RMSE) between experimental data and theoretical curve. More specifically, the procedure has been developed through three refinement steps. In the first one the following range values of the moduli have been explored: $\mu = (5 \div 1000) \times 10^{-4}\ Pas$ and $\mu_{NL} = (5 \div 1000) \times 10^{-7}\ Ns/mm^{6-\alpha}$. The moduli have been progressively increased by $\Delta\mu = 5 \times 10^{-4}\ Pas$ and $\Delta\mu_{NL} = 5 \times 10^{-7}\ Ns/mm^{6-\alpha}$, respectively. The lowest values were chosen in a way such that magnitude of the maximume velocity in the theoretical profile was about some tenths larger then the maximum experimental velocity. As for the order α, in the first refinement step it has been varied in the range $\alpha = 0 \div 1$ at intervals $\Delta\alpha = 0.05$. In the second refinement step the mechanical parameters have been varied with smaller interval in smaller ranges around the values giving the minimum RMSE in the previous step. The same has been done when passing from the second to the third step. The procedure of each refinement step was completely automatic and performed by means of a custom subroutine in Matlab [33]. Between one refinement step and the successive the range and the interval amplitude of parameters have been updated manually. Results of the best fitting are reported in Table 1 and theoretical curves are contrasted with experimental data in Fig. 8. From this figure it is evident that the classical Hagen-Poiseuille model is

Table 1 Parameters obtained by the best-fitting procedure for the HP, Casson and NLHP model.

Model	μ (Pa s)	τ_0 (Pa)	μ_{NL} (Ns/mm$^{6-\alpha}$)	α
HP	1.23×10^{-2}	–	–	–
Casson	2.45×10^{-3}	1.79	–	–
FHP	5.36×10^{-3}	–	7.8×10^{-5}	0.042

not capable of simulating the blood flow in small arterial vessels; the Casson and the proposed fractional nonlocal models, instead, are suitable for simulate the characteristics flattened velocity profiles that are experimentally observed. Some differences, however, may be highlighted between these last two models. While the Casson model has two different behaviors along the diameter, the latter provides a velocity profile that varies very gradually. In order to numerically assess the accuracy of the three models, the RMSE is used. This quantity is defined as:

$$RMSE = \sqrt{\frac{\sum_i^n \left(v_T(x_i) - v_{m,i}\right)^2}{n}} \tag{30}$$

where n is the number of velocity data along the diameter, v_T is the theoretical velocity and v_m is the measured velocity. In Table 2 the RMSEs of the three models are compared. From Table 2 it may be concluded that the proposed nonlocal model

Table 2 Comparison of the RMSEs obtained with the three models HP, Casson and FHP.

Model	RMSE
HP	0.6644
Casson	0.4486
FHP	0.3937

represents an improvement, in terms of accuracy, of results obtained with the Casson model. Then we can state that the proposed nonlocal model is a linear model that is capable to simulate an apparent nonlinearity in the blood behavior. Moreover, it can

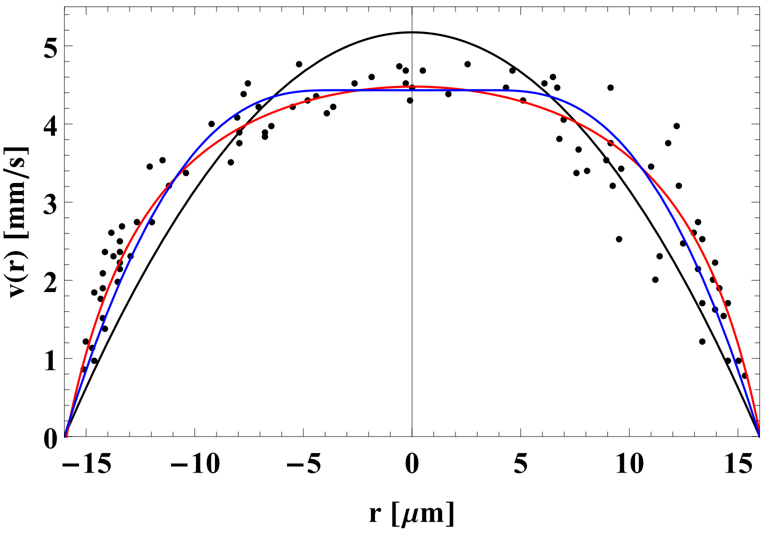

Fig. 8 Comparison between theoretical velocity profile and experimental data (black dots). HP model black line, Casson model blue line, FHP model red line.

be easily verified that another desirable feature of the proposed model is that as the diameter of the vessel increases, nonlocal forces become negligible and the model reverts to the classical Hagen-Poiseuille model. The proposed model, indeed, is size dependent. In order to highlight this concept, in Fig. 9 velocity profiles obtained for different values of the diameter dimensions are compared. Each profile is normalized with respect to the maximum velocity value obtained, for the same diameter value, with the classical HP model ($v_l(0)$). It is easy to note that for relatively large diameter the velocity profile tends to the local response, characterized by a parabolic velocity profile. In contrast, as the diameter of the vessel decreases, the velocity profile becomes flatter and the ratio between the maximum non-local velocity magnitude and the maximum local velocity magnitude becomes smaller and tends to unity.

4 Shear thinning of blood in coaxial cylinder viscometer

An important feature of the rheological behavior of blood is the so-called shear thinning. This effect has been observed experimentally from decades and it regards the decrease of apparent viscosity of blood for increasing shear rate. It is widely believed that the shear thinning of blood is due mainly to the deformability of RBCs ([34]). This hypothesis is particularly suitable for the mesoscale approach adopted in this paper; indeed, in [34] measurements in a coaxial cylinder viscometer have been performed with three types of suspension: normal RBC in heparinized plasma, normal RBC in 11% albumin-Ringer solution and hardened RBC in 11% albumin-Ringer solution. It has been shown that only the suspension with hardened RBC shows an almost constant viscosity for varying shear rate, while the other suspensions show a clear shear thinning effect, expecially for normal RBC in plasma (see Fig. 1 of [34])

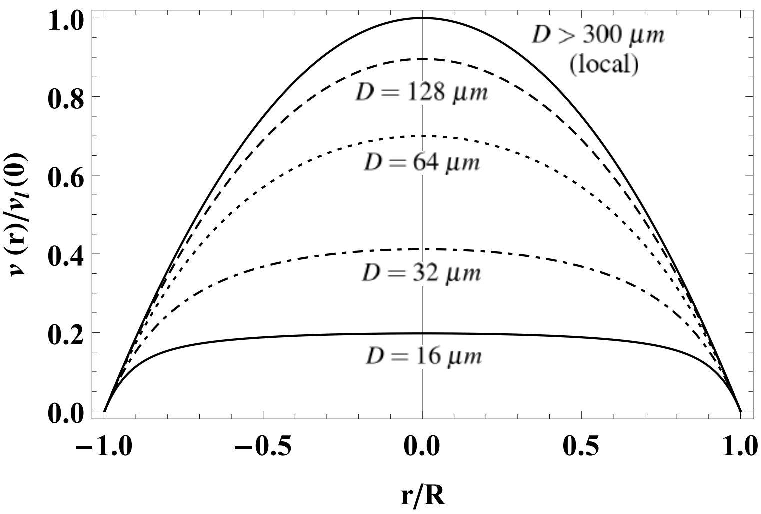

Fig. 9 Size effect of the fractional non-local Hagen-Poiseuille model.

In the frame of a mesoscale approach of this work, it is easy to hypothesize a qualitative mechanism that, as a consequence of RBC deformability, is responsible of the shear thinning when blood viscosity is measured in a coaxial cylinder viscometer. Indeed in such a kind of viscometer the (apparent) shear rate is directly proportional to the angular velocity of the moving cylinder; the shear rate is apparent because no assumption has been made on the rheological behavior of blood, then the velocity profile is implicitly assumed linear and the apparent (constant) shear rate $\dot{\gamma}_a$ is evaluated simply as:

$$\dot{\gamma}_a = \frac{\omega R_i}{R_e - R_i} \tag{31}$$

where ω is the angular velocity of the internal cylinder, R_e and R_i are the external and internal radius of the chamber where the blood is placed for the measurement, respectively; in Eq. (31) the external cylinder is not rotating. As a consequence of the fact that the shear rate is apparent, the viscosity values reported in [34] are apparent as well.

The role played by the deformability of RBCs is clearly illustrated in Fig. 10; as ω increases, the inertial forces increase and as results RBCs migrate to the external cylinder surface; moreover, as they aggregate to the internal surface of the external cylinder, they are flattened by inertial forces. The distribution and shape of RBCs are sensibly different from one value of ω to another and as a consequence macroscopic rheologic behavior of blood is changed.

For these reasons, in the following we reinterpreted the data published in [34] by using the proposed rheological model. In a coaxial cylinder viscometer the tangential stress measurement is obtained indirectly from the measure of the torque M_T applied by the blood to the rotating (internal) cylinder:

$$\tau = \frac{M_T}{2\pi R_i^2 H} \tag{32}$$

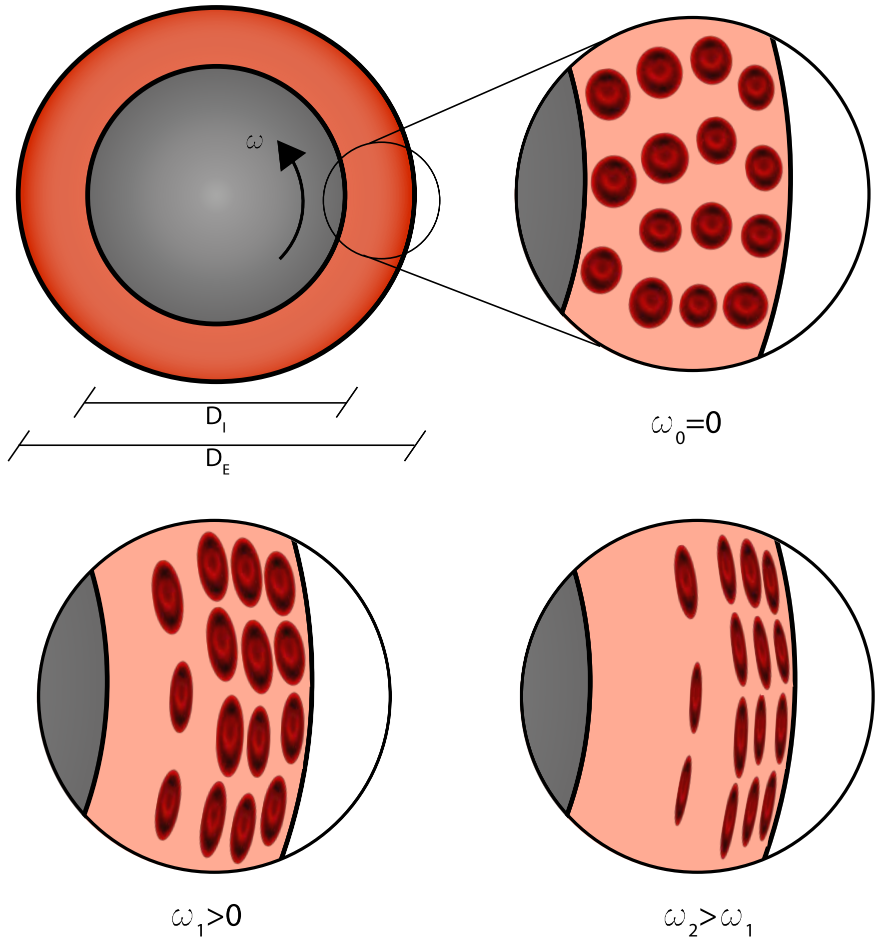

Fig. 10 Mesoscale explanation of the shear thinning of blood in the double cylinder rheometer as a consequence of deformability of RBC.

being H the height of the internal cylinder. The apparent viscosity is then evaluated simply as:

$$\mu_a = \frac{\tau}{\dot{\gamma}_a} \tag{33}$$

The parameters of the nonlocal model proposed here have been optimized for several couples of values of shear rate and viscosity deducted from [34]; the parameters have been tuned in such way that for each apparent shear rate value $\dot{\gamma}_a$ the tangential stress obtained with the proposed model is equal to the tangential stress obtained by multiplying the value of shear rate and viscosity in [34]; to this purpose the data related to normal RBC in plasma have been considered. In Fig. 11 the shear stress versus the apparent shear strain, obtained from data in [34] is depicted. In order to optimize the parameters of the proposed nonlocal model, numerical simulations of

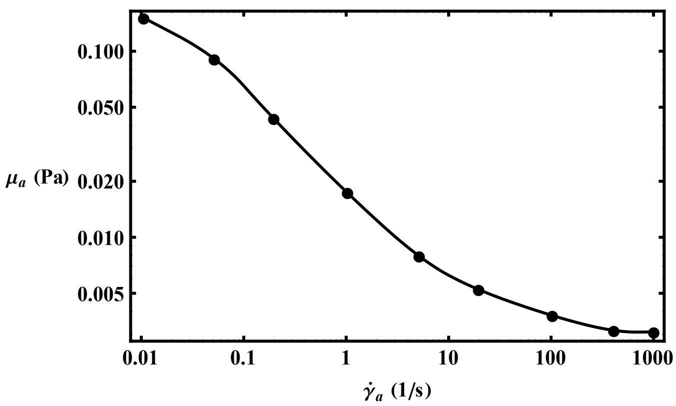

Fig. 11 Apparent viscosity as a function of apparent shear rate experimental data (dots) and proposed nonlocal model (continuous line)

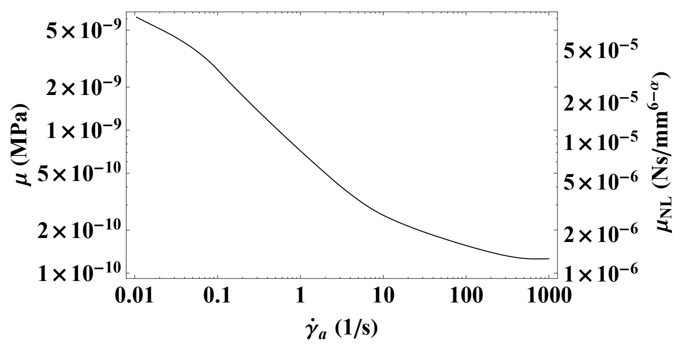

Fig. 12 Local and nonlocal viscosity parameters μ and μ_{NL} as a function of apparent shear rate for the proposed nonlocal model.

the conditions inside the coaxial cylinder viscometer have been performed. To this purpose, the geometry of the viscometer has been considered equal to that of a commercial viscometer, that is $R_i = 17.245$ mm ad $R_e = 18.415$ mm. In the optimization procedure, only the parameters μ and μ_{NL} have been calibrated, while the parameter α has been assumed equal to the value obtained by the best fitting procedure based on the velocity profile data and described in the previous section. For each experimental value coming form the rotating viscometer, the parameters μ and μ_{NL} have been calibrated iteratively as done in Section 3.3 for the Poiseuille flow. By means of this optimization procedure, we have been able to reproduce the experimental data obtained in [34] in terms of apparent shear rate and apparent viscosity, as shown in Fig. 11. In order to obtain these results, the coefficients μ and μ_{NL} varies with the apparent viscosity with the same trend of the apparent viscosity, as shown in Fig. 12 (continuous thick line). From the values of Fig. 11 the curve of the shear stress vs the apparent shear rate have been obtained. Indeed in Fig. 13 the shear stress-apparent shear rate curve obtained for the blood have been contrasted with a linear behavior tangent to the blood curve at its lowest shear rate value. It is clear that, especially for low values of the apparent shear rate, the behavior of blood is nonlinear, indeed as the apparent shear rate increases the shear stress grows less than linearly. In order to show the capability of the proposed model, in Fig. 13 it is also shown a curve related to a hypothetical fluid with a shear thickening behavior, that is a behavior opposite to that of blood.

5 Conclusion

In this paper a nonlocal model for the blood behavior in small arterial vessels has been introduced. The model is based on a mesoscale approach in which the presence of RBCs and other cells dispersed in the blood plasma is neglected but taken into account in the rheological behavior of blood by adding long-range interactions between non-adjacent fluid elements in the equilibrium equations. The use of a power law attenuation function leads to governing equations involving fractional derivatives in case of unbounded domains or operator closely related to the fractional ones in case of bounded domains. The model has proved to be very efficient in reproducing experimental velocity profiles without the need of nonlinearity in the rheological behavior. In comparison with existing non local models one important property of the proposed nonlocal model is that boundary conditions may be enforced as in a local model. To this stage, the only negative aspect of the proposed formulation is that it has not been possible to obtain an analytical solution for the considered application that would be desirable for a straightforward tuning of the mechanical parameters. However, despite this undesirable feature, in the future the model maybe applied to more complicated problems and implemented in a CFD context, where the knowledge of analytical solutions is not required.

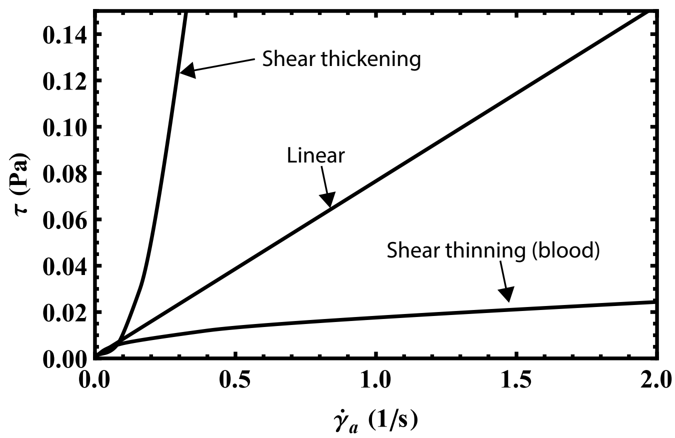

Fig. 13 Shear thinning of blood and hypothetical shear thickening behavior obtained with the proposed model.

Appendix - Fractional calculus

In this section, a brief introduction to the fundamentals of fractional calculus will be given.

Consider the function $f(x)$, $x \in \mathbb{R}$, the left and the right Riemann-Liouville (RL) fractional integral are defined as [25]:

$$\left(I_{+}^{\alpha} f\right)(x) = \frac{1}{\Gamma(\alpha)} \int_{-\infty}^{x} \frac{f(\xi)}{(x-\xi)^{1-\alpha}} d\xi \tag{34a}$$

$$\left(I_{-}^{\alpha} f\right)(x) = \frac{1}{\Gamma(\alpha)} \int_{x}^{\infty} \frac{f(\xi)}{(\xi-x)^{1-\alpha}} d\xi \tag{34b}$$

while the RL fractional derivative are defined as:

$$\left(D_{+}^{\alpha} f\right)(x) = \frac{1}{\Gamma(1-\alpha)} \frac{d}{dx} \int_{-\infty}^{x} \frac{f(\xi)}{(x-\xi)^{\alpha}} d\xi \tag{35a}$$

$$\left(D_{-}^{\alpha} f\right)(x) = -\frac{1}{\Gamma(1-\alpha)} \frac{d}{dx} \int_{x}^{\infty} \frac{f(\xi)}{(\xi-x)^{\alpha}} d\xi \tag{35b}$$

where $\alpha \in \mathbb{R}$, $0 \leq \alpha \leq 1$ and $\Gamma(\cdot)$ is the Euler gamma function. If $f(x)$ is a continuous function with continuous first derivative, the left and right RL fractional derivatives are coincident with the Marchaud fractional derivatives, that may be written as follows:

$$\left(\mathbf{D}_{+}^{\alpha} f\right)(x) = \frac{\alpha}{\Gamma(1-\alpha)} \int_{-\infty}^{x} \frac{f(x)-f(\xi)}{(x-\xi)^{\alpha}} d\xi \tag{36a}$$

$$\left(\mathbf{D}_{-}^{\alpha} f\right)(x) = \frac{\alpha}{\Gamma(1-\alpha)} \int_{x}^{\infty} \frac{f(x)-f(\xi)}{(\xi-x)^{\alpha}} d\xi \tag{36b}$$

The Marchaud fractional derivatives may be defined also for a bounded domain $0 \leq x \leq L$ as:

$$\left(\mathbf{D}_{0^{+}}^{\alpha} f\right)(x) = \frac{\alpha}{\Gamma(1-\alpha)} \int_{0}^{x} \frac{f(x)-f(\xi)}{(x-\xi)^{1+\alpha}} d\xi + \frac{f(x)}{\Gamma(1-\alpha) x^{1+\alpha}} \tag{37a}$$

$$\left(\mathbf{D}_{L^{-}}^{\alpha} f\right)(x) = \frac{\alpha}{\Gamma(1-\alpha)} \int_{x}^{L} \frac{f(x)-f(\xi)}{(\xi-x)^{1+\alpha}} d\xi + \frac{f(x)}{\Gamma(1-\alpha)(L-x)^{1+\alpha}} \tag{37b}$$

The definitions of Marchaud fractional derivatives related to a single-variable scalar function may be extended to a multi-variable scalar function. The extension is more readable if referred to the Riesz fractional operators. Then it is necessary to introduce Riesz fractional integral $(\bar{I}^{\alpha} f)(x)$ and derivative $(\bar{D}^{\alpha} f)(x)$:

$$(\bar{I}^{\alpha} f)(x) = \nu(\alpha) \int_{-\infty}^{\infty} \frac{f(\xi)}{|x-\xi|^{1-\alpha}} d\xi = \nu(\alpha) \left[\left(I_{+}^{\alpha} f\right)(x) + \left(I_{-}^{\alpha} f\right)(x) \right] \tag{38a}$$

$$\begin{aligned}(\bar{D}^{\alpha} f)(x) = \nu(-\alpha) \int_{-\infty}^{\infty} \frac{f(x-\xi)-f(x)}{|\xi|^{1+\alpha}} d\xi = \\ = \Gamma(1-\alpha)\nu(-\alpha) \left[\left(\mathbf{D}_{+}^{\alpha} f\right)(x) + \left(\mathbf{D}_{-}^{\alpha} f\right)(x) \right]\end{aligned} \tag{38b}$$

where $\nu(\pm\alpha) = [2\cos(\alpha\pi/2)\Gamma(\pm\alpha)]^{-1}$. The Riesz fractional operator may be generalized to multivariate scalar function $f(\mathbf{x})$, with $\mathbf{x} \in \mathbb{R}^n$:

$$\left(\bar{D}^{\alpha} f\right)(\mathbf{x}) = \frac{1}{d_{n,\bar{l}}(\bar{\alpha})} \int_{\mathbb{R}^n} \frac{f(\boldsymbol{\xi}) - f(\mathbf{x})}{||\boldsymbol{\xi} - \mathbf{x}||^{n+\alpha}} d\boldsymbol{\xi} = \frac{\chi(\bar{\alpha})}{d_{n,\bar{l}}(\bar{\alpha})} \left[\left(\mathbf{D}_{+}^{\alpha} f\right)(\mathbf{x}) + \left(\mathbf{D}_{-}^{\alpha} f\right)(\boldsymbol{x})\right] \quad (39)$$

where:

$$d_{n,l}(\alpha) = \beta_n(\alpha) \frac{A_l(\alpha)}{\sin(\alpha\pi/2)} \quad (40a)$$

$$\beta_n(\alpha) = \frac{\pi^{1+n/2}}{2^{\alpha}\Gamma(1+\alpha/2)\Gamma(n+\alpha/2)} \quad (40b)$$

$$A_l(\alpha) = \sum_{k=0}^{l} (-1)^{k-1} \binom{l}{k} k^{\alpha} \quad (40c)$$

and $\chi_l(\alpha) = -A_l(\alpha)\Gamma(\alpha)$, $\bar{\alpha} = n-1+\alpha$, $\bar{l} = n-1+l$, $l = \{\alpha\}+1$ and $\{\alpha\}$ is the integer part of α. The complete demonstration of Eq. (39) is omitted here for the sake of brevity; more information can be found in [26].
Finally, we briefly introduce the n-dimensional Central Marchaud Fractional Derivative (CMFD) as:

$$\left(\mathbf{D}_{-}^{\alpha} f\right)(\boldsymbol{x}) = \frac{\alpha}{\Gamma(1-\alpha)} \int_{\mathbb{R}^n} \frac{f(\boldsymbol{x}) - f(\boldsymbol{\xi})}{(\boldsymbol{\xi} - \boldsymbol{x})^{n+\alpha}} \boldsymbol{J}_{kj} d\boldsymbol{\xi} \quad (41)$$

where $\boldsymbol{J}_{kj} = \boldsymbol{i}_k \boldsymbol{i}_j$ is a Jacoby directional tensor, being $\boldsymbol{i}_k$ the unit vector associated with the direction $\boldsymbol{x} - \boldsymbol{\xi}$. In the specific problem treated in this paper (the Poiseuille flow), the governing equation written in polar coordinates and in axisymmetric conditions is basically a scalar governing equation, then the Jacoby tensor reduce to unity. This means that the power law attenuation function, responsible for the appearance of fractional operator, reduces in this case to a scalar function. As a consequence, in the governing equation in Eq. (29), the integral term may be recognized as the integral part of the Marchaud fractional derivative defined in bounded domain and reported in Eq. (37). More details can be found in [31].

Funding

Thuis study was not founded.

Conflict of interest

The authors declare that they have no conflict of interest.

References

1. Fung, Y.C. (1999). *Biomechanics - Circulation*, New York: Springer-Verlag.
2. Venkatesan, J., Sankar, D.S., Hemalatha, K., Yatim, Y. (2013). Mathematical Analysis of Casson Fluid Model for Blood Rheology in Stenosed Narrow Arteries. *Journal of Applied Mathematics*, 2013, 1-13.
3. Tangelder, G.J., Slaaf, D.W., Muijtjens, A.M.M., Arts, T., Egbrink, M.G.A., Reneman, R.S. (1986). Velocity profiles of blood platelets and red blood cells flowing in arterioles of the rabbit mesentery. *Circulation Research*, 59(5), 505-514.
4. Lam, D.C.C., Yang, F., Chong, A.C.M., Wang, J., Tong, P. (2003). Experiments and theory in strain gradient elasticity. *Journal of the Mechanics and Physics of Solids*, 51(8), 1477-1508.
5. Lu, X., Bardet, J.P., Huang, M. (2009). Numerical solutions of strain localization with nonlocal softening plasticity. *Computer Methods in applied mechanics and engineering*, 198, 3702-3711.
6. Ebrahimi, F., Barati, M.R., Dabbagh, A. (2016). A nonlocal strain gradient theory for wave propagation analysis in temperature-dependent inhomogeneous nanoplates. *International journal of engineering science*, 107, 169-182.
7. Lim, C.W., Zhang, G., Reddy, J.N. (2015). A higher-order nonlocal elasticity and strain gradient theory and its applications in wave propagation. *Journal of the mechanics and physics of solids*, 78, 298-313.
8. Eringen, A.C. (1972). Linear theory of nonlocal elasticity and dispersion of plane waves. *International Journal of Engineering Science*, 10, 425-435.
9. Koutsoumaris, C.C., Eptaimeros, K.G., Tsamasphyros, G.J. (2017). A different approach to Eringen's nonlocal integral stress model with applications for beams. *International Journal of Solids and Structures*, 112, 222-238.
10. Silling, S.A. (2000). Reformulation of elasticity theory for discontinuities and long-range forces. *Journal of the Mechanics and Physics of Solids*, 48, 175-209.
11. Tordesillas, A., Peters, J.F., Gardiner, B.S. (2004). Shear band evolution and accumulated microstructural development in Cosserat media. *International journal for numerical and analytical methods in geomechanics*, 28, 981-1010.
12. Bordignon, N., Piccolroaz, A., Dal Corso, F., Bigoni, D. (2015). Strain localization and shear banding in ductile materials. *Frontiers in Materials*, 2, 1-13.
13. El-Nabulsi, R.A. (2017). Dynamics of pulsatile flows through microtubes from nonlocality. *Mechanics research communications*, 86, 18-26.
14. Owens, R.G. (2006). A new microstructure-based constitutive model for human blood. *Journal of Non-Newtonian fluid mechanics*, 140, 57-70.
15. Fang, J., Owens, R.G. (2006). Numerical simulations of pulsatile blood flow using a new constitutive model. *Biorheology*, 43(5), 637-660.
16. Drapaca, C.S. (2018). Poiseuille flow of a nonlocal non-newtonian fluid with wall slip: a first step in modeling cerebral microaneurysms. *Fractal and fractional*, 2(9), 1-20.
17. Van, P., Fulop, T. (2006). Weakly nonlocal fluid mechanics: Schrodinger equation. *Proceedings of the royal society A*, 462, 541–557.
18. Todd, B.D., Hansen, J.S. (2008). Nonlocal viscous transport and the effect on fluid stress. *Physical review E*, 78, 051202.
19. Di Paola, M., Failla, G., Zingales, M. (2009). Physically-based approach to the mechanics of strong nonlocal linear elasticity theory. *Journal of elasticity*, 97(2), 103-130.
20. Di Paola, M., Failla, G., Zingales, M. (2013). Non-local stiffness and damping models for shear-deformable beams. *European Journal of Mechanics, A/Solids*, 40, 69–83.
21. Di Paola, M., Failla, G., Pirrotta, A., Sofi, A., Zingales, M. (2013). The mechanically based nonlocal elasticity: An overview of main results and future challenges. *Philosophical Transactions of the Royal Society A: Mathematical, Physical and Engineering Sciences*, 371, 20120433.
22. Alotta, G., Failla, G., Zingales, M. (2014). Finite element method for a nonlocal Timoshenko beam model. *Finite element in analysis and design*, 89, 77-92.
23. Alotta, G., Failla, G., Zingales, M. (2017). Finite element formulation of a nonlocal hereditary fractional order Timoshenko beam. *Journal of Engineering Mechanics - ASCE*, 143(5), D4015001.
24. Alotta, G., Di Paola, M., Failla, G., Pinnola, F.P. (2018). On the dynamics of nonlocal fractional viscoelastic beams under stochastic agencies. *Composites Part B*, 137, 102-110.
25. Podlubny, I. (1999). *Fractional differential equation*. San Diego: Academic Press.
26. Samko, S.G., Kilbas, A.A., Marichev, O.I. (1993). *Fractional Integral and Derivatives*. Amsterdam: Gordon&Breach Science Publisher.
27. Aifantis, E.C. (2003). Update on a class of gradient theories. *Mechanics of Materials*, 35, 259-280.

28. Li, L., Hu, Y. (2016). Wave propagation in fluid conveying viscoelastic carbon nanotubes based on nonlocal strain gradient theory. *Computer material science*, 112, 282-288.
29. Perrot, A., Challamel, N., Picandet, V. (2014). Poisueille flow of nonlocal microstructured fluid. *Mechanics Research Communications*, 59, 51-57.
30. Romano, G., Barretta, R. (2017). Stress-driven versus strain-driven nonlocal integral model for elastic nano-beams. *Composites Part B*, 114, 184-188.
31. Di Paola, M., Zingales, M. (2011). Fractional differential calculus for 3D mechanically based nonlocal elasticity. *International Journal for Multiscale Computational Engineering*, 9(5), 579-597.
32. Carpinteri, A., Cornetti, P., Sapora, A. (2014). Nonlocal elasticity: an approach based on fractional calculus. *Meccanica* (2014), 49, 2551-2569.
33. MATLAB 2018a, The MathWorks Inc., Natick, Massachusetts, United States.
34. Chien, S. (1970). Shear dependence of effective cell volume as a determinant of blood viscosity. *Science*, 168, 977-979.